REPORT

MEMS-BASED SCANNING CALORIMETER FOR THERMODYNAMIC PROPERTIES OF NANOSTRUCTURES

L. H. Allen and S. L. Lai
Materials Science and Engineering, University of Illinois, Urbana, Illinois, USA

Thermodynamic properties of small structures, such as the melting points and the process of mass transport, can be considerably different compared to material in the bulk form. Calorimetry is the standard experimental technique used to measure thermodynamics properties. However, this technique is extremely difficult to use for the study of small structures because the amount of energy exchanged during the measurement is extremely small—proportional to the amount of material. In order to measure small amounts of thermal energy we have scaled down the physical size of the calorimeter using MEMS technology. This thin-film differential scanning calorimeter has extremely high sensitivity, $\sim 0.01\ mJ/cm^2$, and is capable of measuring the melting phenomenon of 1 Å of Sn deposited onto a SiN surface. In this article we investigate the size dependence of both the melting point and the heat of fusion for ultrathin films of Sn nanonstructures using multiple evaporation and thermal annealing cycles.

Interest in the thermodynamic properties of small particles began over a hundred years ago with Gibbs, who considered the affect of the surface on the bulk properties of material and suggested that the melting point T_m of small particles could be much lower than that of bulk materials. Not only does the surface alter the thermodynamic properties of material on the nanometer scale, it also plays a key role in the dynamic process of material transport such as the coalescence of clusters during the early stages of thin-film growth.

There has been much progress in studying the thermodynamics of small structures: the size-dependent melting-point depression has been observed experimentally [1] using transmission electron microscopy (TEM) techniques, and computational efforts in model systems such as Au have been advanced showing that nanoscale material simultaneously displays both solidlike and liquidlike characteristics and time-dependent structural instabilities [2–4].

Received 12 August 1997; accepted 8 September 1997

We gratefully acknowledge P. Infante of the Cornell Nanofabrication Facility (CNF) at Cornell University for technical support. This work is financially supported by the National Science Foundation (NSF DMR 94-19604) and the Joint Service Electronics Program (JESP N00014-90-1-129). Microanalysis and microstructural characterization were performed at the Center for Microanalysis, University of Illinois, supported by the U.S. Department of Energy under grant DEFG 02-91ER35439.

Address correspondence to L. H. Allen, 1304 West Green Street, Department of Materials Science and Engineering, University of Illinois, Urbana, IL 61801, US. E-mail: l-allen9@uiuc.edu

Microscale Thermophysical Engineering, 2:11–19, 1998

1089-3954/98 $12.00 + .00

There are many techniques for studying the structural characterization of nanostructures (e.g., TEM, SEM, AFM, STM, RDX, etc.). However, thermodynamics studies using the measurement of the energy at the nanojoule scale are extremely rare due to the lack of experimental techniques. The ideal technique for the measurement for many thermodynamic properties is calorimetry. However, current conventional calorimetry lacks the sensitivity ($\sim$ 50 mJ/cm^2) to measure the minuscule amounts of energy generated for typical samples of nanostructures or buried silicide nuclei.

Currently, conventional differential scanning calorimetry (DSC) systems, such as the Perkin Elmer DSC-2 system, are often used for measuring the enthalpy of reactions such as crystallization of amorphous materials and bilayer reaction couples. Unfortunately, these systems have been traditionally designed for large bulk samples (milligrams) and are usually not sensitive enough for thin-film samples (nanograms), where the amount of heat generated during the reaction is extremely small and is marked by the large heat capacity of the calorimeter apparatus. For example, in order to measure the homogeneous and interface crystallization energy of α-Si using DSC, Donovan et al. [5] were required to fabricate and then stack extremely thick samples ($\sim$ 120,000 Å), so that the heat which was generated was large enough to be measured by the calorimeter.

In the mid-1980s, Spaepen, Thompson, Clevenger, Cotts, Johnson, and Harper pioneered the use of DSC for ex-situ thin film work by making special multilayer samples with a thickness of about 1,000 Å [6–8]. This allowed calorimetry studies of interface reaction at a level far superior than before. However, the intrinsic sensitivity of the calorimeter itself has not improved and still remains in the equivalent range of 50–500 mJ/cm^2. In order to advance calorimetry from a "bulk" to a "surface" probe, the basic sensitivity of the calorimeter must be increased.

We have recently made advances in calorimetry technique [9–12] by designing a thin-film differential scanning calorimetry (TDSC) device. It has extremely high sensitivity, $\sim$ 0.01 mJ/cm^2, an ultrafast scanning rate of up to $10^{6\circ}$C/s, and a wide range in operating temperature extending up to 700°C. The TDSC device is used in situ within an ultrahigh vacuum system allowing for rigid control of sample preparation conditions. We have begun to study the thermodynamic properties of nanostructures on a free surface. Using the nanocalorimetry technique we observed evidence of a size-dependent reduction of both T_m and H_m [9].

Two key features of our scanning calorimeter include the reduction of the overall thermal mass [13–18] of the calorimetry system and the use of a fast scan rate. The ability to measure small amounts of heat depends on the relative heat capacity of the entire calorimetry apparatus. By reducing the thermal mass of the apparatus, the sensitivity can be increased dramatically. The scan rate in calorimetry is important because sensitivity is related to the heat loss during the measurement. In our design, the high heating rate ($10^3 \rightarrow 10^{6\circ}$C/s) during the scan is far greater than the cooling rate of the system, thus the system approaches a quasi-adiabatic condition.

By utilizing standard thin-film membrane processing technology developed at Cornell University, we have combined the four components typically found in a calorimetry system, namely, the sample, the sample holder, the heater, and the

thermometer, into a single multilayer thin-film configuration, as shown in Figure 1. In this design, the sample holder is a thin, 500-Å SiN membrane window supported at the perimeter by the Si substrate. A thin, 200-Å Ni stripe on the membrane is the key element of the calorimeter and functions both as a resistance microheater and a thermistor. The material of interest is deposited on the opposite side of the membrane. The membrane ensures good thermal conduction between the sample and heater, while it isolates them electrically.

Our calorimetry measurement is initiated by supplying a short, ~ 10-ms dc current pulse to the Ni stripe, thus raising the temperature of the system by joule heating, as described by our earlier work in the development of the microheater technique [12]. The voltage and current are monitored in real time during the pulse and thus the power supplied to the quasi-adiabatic system is obtained directly ($P = VI$). At these fast heating rates the temperature of the microheater system is determined by measuring the changes in resistance, $R = V/I$, of the metal strip. The intrinsic values for thermal coefficient of resistance (TCR) characteristics of the Ni heater/thermistor are calibrated beforehand using a conventional vacuum tube furnace and with a calibrated thermocouple.

In order to evaluate the data in terms of standard thermodynamic parameters the raw data are evaluated in terms of the heat capacity C_p. This is obtained from the data using the following expression:

$$C_p = \frac{dQ/dt}{dT/dt} = \frac{V(t)*I(t)}{dT/dt} \tag{1}$$

C_p is plotted as a function of temperature, as shown in Figure 2 for a set of samples with various amounts of Sn. The temperature at the peak of each scan represents the melting point of the sample, whereas the integrated area under the peak represents the heat of fusion.

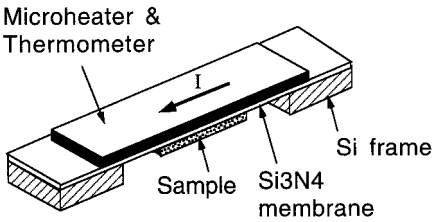

Figure 1. Sketch of MEMS-based thin-film scanning calorimeter. The mechanical base of the entire device is a standard Si wafer that has been coated with a thin film of SiN. A SiN window is then formed by selectively etching the Si from the bottom side of the wafer with standard KOH solution. A SiN membrane provides mechanical support for the microheater, as well as a chemical and electrical barrier between the heater and sample. A thin film of metal functions acts as both heater and thermistor. The SiN membrane can eventually be removed, leaving a thin metal membrane. By putting two microheater devices together side by side, the system can be configured to make a highly sensitive thin-film differential scanning calorimeter (TDSC).

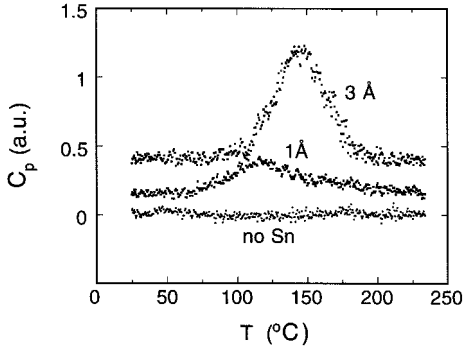

Figure 2. Heat capacity results during a TDSC scan of 1 Å and 3 Å of Sn. For these small amounts of thermally deposited material, the layers become discontinuous. The Sn immediately coalesces, forming small three-dimensional (spherical) particles with a distribution of sizes having radii of the scale of nanometers. The position of the peak height represents the average melting point of the distribution. For each deposition cycle there is a range of sizes of particle radii. Since there is a size dependence of the melting point of the particles, there is a broad temperature range over which the ensemble of particles melts. The area under the peak represents the energy needed to melt the nanostructure material.

In this study Sn nanometer-size particles were formed by successive deposition (~ 1 Å/s) of pure Sn onto the SiN side of the thin-film scanning calorimeter using the thermal evaporation. For the small amounts of Sn deposited here, the films are discontinuous and form self-assembled nanometer-sized islands on the inert substrate. In contrast to embedding metal-precipitated particles in a bulk matrix [19, 20], this type of sample preparation produces spherical Sn particles of high purity and stress-free surface conditions, which are ideal for this melting study.

Calorimetric measurements were performed immediately after each deposition at a base pressure of $\sim 1 \times 10^{-8}$ torr. Since the TDSC device is extremely thin, the entire TDSC sample including the microheater/nanostructures were separated from the Si wafer and were immediately available for TEM analysis. The particle size was measured using a Phillips CM-12 TEM. The mean radius is hereafter taken as the Sn particle size.

An example of a typical TDSC result is shown in Figure 2 for two experiments where extremely small amounts of Sn, 1 Å and 3 Å of Sn, were deposited. Note the shift in melting point. Analysis of the C_p data yields the values for ΔH_m and T_m for the various sizes of Sn particles. The average melting temperature and normalized heat of fusion are plotted in Figures 3 and 4. For bulk Sn, the melting point is 232°C [21]. It is evident that the melting points decrease systematically as the size of Sn particles decreases, a reduction of over 100°C. This phenomenon has also been observed by Wronski [22]. The depression of melting temperature was confirmed during the course of this work by using TEM diffraction techniques during in-situ heating of the Sn samples deposited on amorphous carbon films.

The classical theory of Hanszen [23] analyzed the melting temperature in terms of liquid-shell model. In this model he assumes that a solid particle is embedded in a thin liquid overlayer and the melting temperature is taken to be the temperature of equilibrium between the solid sphere core and the liquid overlayer.

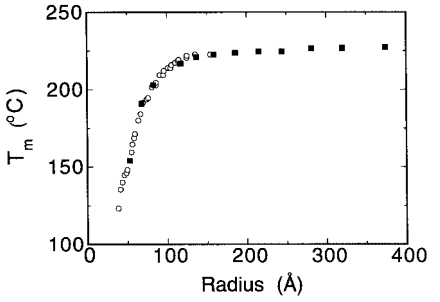

Figure 3. Melting-point data for Sn clusters as a function of size of cluster. The data are the superposition of four different multiple evaporation/annealing experiments (A = 1 Å, B = 2 Å, C = 4 Å, and D = 6 Å). For example, for the A series experiment, 1 Å was evaporated followed by a TDSC 300°C anneal and then the cycle was repeated by again depositing another 1 Å, and so on.

The critical thickness t_0 of the liquid shell is an adjustable parameter in accordance with the experimental results. The melting points T_m of Sn particles with radius r is expressed as

$$T_0 - T_m = \frac{2T_0}{\Delta H_0}\left[\frac{\sigma_s}{\rho_s(r - t_0)} + \left(\frac{\sigma_l}{r} + \frac{\Delta P}{2}\right)\left(\frac{1}{\rho_s} - \frac{1}{\rho_l}\right)\right] \tag{2}$$

where T_0 is the bulk melting temperature of solid Sn and ΔH_0 is its latent heat of fusion; σ_s and σ_l are the interfacial surface tensions between the solid and the liquid and between the liquid and its vapor respectively, and ρ_s and ρ_l are the densities of the solid and liquid, respectively; t_0 is the critical thickness of liquid layer at T_m. ΔP is the difference between the vapor pressure at the surface of the liquid layer with an outer radius r at T_m and the vapor pressure at the flat liquid surface ($r = \infty$) at T_0. It has been shown that ΔP can be neglected for Sn [22]. Substituting $T_0 = 232$°C, $\rho_s = 7.18$ g/cm^3, $\rho_l = 6.98$ g/cm^3 [22], $\sigma_l = 550$ mN/m [24], and $\sigma_s = 54.5$ mN/m [25] into Eq. (2), we obtain the following expression:

$$T_m = 232 - 782\left[\frac{\sigma_s}{15.8(r - t)} - \frac{1}{r}\right] \tag{3}$$

From our experimental data we obtain a value of $t_0 = 18$ Å for the liquid overlayer thickness. Using optical techniques [26], the existence of a liquid layer on

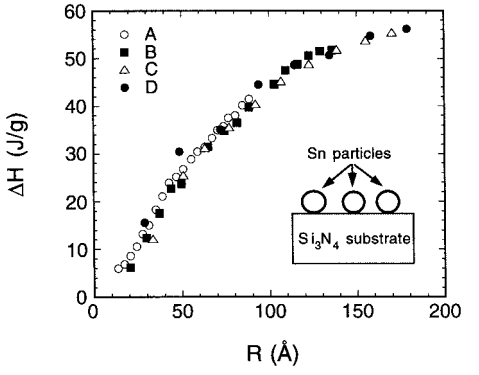

Figure 4. Heat of fusion data for Sn clusters as a function of size of cluster. The data are the superposition of four different multiple evporation/anneal experiments (A = 1 Å, B = 2 Å, C = 4 Å, and D = 6 Å).

the surface of nanometer-size Pb particles prior to the complete melting of the bulk material has been shown. In addition, computational simulations have also shown the liquidlike precursor prior to the complete melting of small Au particles [27]. The formation of a molten surface overlayer equilibrating with the solid core is related directly to the surface melting phenomenon. For example, the Pb [28] and Al [29] surfaces of bulk crystals have been observed to melt at temperatures below the bulk melting temperatures, with a continuous increase in the thickness of the melted layer as the temperature approaches the bulk melting point. For small metal particles, the surface melting is strongly enhanced by curvature effects. Observations of clusters [30, 31] show that the surface melting of small clusters/particles occurs over a broader temperature range and that the thickness of the liquid layer is much greater than that observed on bulk crystals.

The measurements of melting-temperature depression have been, until now, the only experimental evidence which supports the liquid shell mode of nanostructures on free surfaces. Is this enough evidence? After all, for conventional bulk material analysis, temperature is an intensive material property and not dependent on the quantity (size) of material. If the liquid shell model is correct, then other material properties associated with the melting process should also be dependent on the size of the particle. The heat of fusion ΔH_m is such a property, and through the following discussion of our nanocalorimetry measurements we deduce that the liquid shell model is indeed a reasonable model.

The normalized heat of fusion ΔH_m as a function of particle size is shown in Figure 4. The data indicate that there is a large decrease in ΔH_m (70%) as compared with the bulk value (58.9 J/g) [21] when the particle size is reduced. From the viewpoint of classical thermodynamics, the latent heat of fusion assumes a constant value. Recently, however, molecular dynamics simulations have shown a size-dependent decrease of ΔH_m with decreasing cluster size (e.g., Au clusters [27]).

In order to relate the heat of fusion to the heat measured by the calorimeter, we must consider the details of the melting process. Surface melting of small particles occurs in a continuous manner over a broad temperature range, whereas the homogenous melting of the solid core occurs abruptly at the critical temperature T_m [31]. The total heat required for both surface and solid core melting is supplied by the calorimeter. However, the heat for the surface melting is supplied over a broad temperature range and appears as a gradual increase ($\sim$ 0.1%) in the background heat capacity of the system, a value which is too small to be measured by our present techniques. Conversely, the heat supplied for the abrupt melting of solid core is measured directly using our technique.

For the purpose of describing quantitatively the heat of fusion for small Sn particles, it is necessary to separate the volumes of the liquid surface layer and the solid core region. We thus define the volume of the spherical liquid shell as an "excluded volume" δV, which is related to the critical thickness t_0 of the liquid layer via the following expression:

$$\delta V = \frac{4}{3}\pi\left[r^3 - (r - t_0)^3\right] \tag{4}$$

Assuming that the latent heat of fusion per volume of the bulklike solid core is independent of temperature, we obtain the corrected values for the normalized heat of fusion in terms of the original particle size r and the thickness of the liquid layer t_0. Using only the heat of fusion data, we obtain an independent value for the thickness of the liquid layer of $t_0 \approx 13$ Å, which agrees well with the values obtained from the melting-point data ($t_0 \approx 18$ Å).

In order to study the growth of clusters, we have also shown (Figures 3 and 4) a set of multiple evaporation/annealing experiments superimposed. In this case we form large clusters or islands by performing multiple evaporation followed by TDSC annealing. Each cycle consists of the deposition of 1, 2, 4, or 6 Å of Sn, immediately followed with multiple thermal annealing (300°C) TDSC pulses. A full set of calorimetry data for $C_p(T, t)$ is acquired during each pulse. By doing the experiment in this way we deposit a blanket layer of atoms onto a surface that already contains large stable three-dimensional clusters. The freshly deposited atoms form many small clusters in the open area between the preexisting islands. In essence, the deposition process supersaturates the open area with Sn atoms. Because of the higher surface/volume ratio, the atoms that make up the clusters have a higher chemical potential than those atoms that form the nearby islands. Therefore, there exists a driving force for the coalescence process. However, at ambient temperatures the diffusion of the atoms is kinetically stalled and thus the small clusters remain intact.

When the sample is heated to high temperatures, which occurs during the first TDSC pulse following deposition, the atoms diffuse from the small clusters toward the islands and the islands grow (coalescence) at the expense of the small clusters. The data indicate that the melting point and heat of fusion of a cluster are controlled only by the size of the particles and are independent of the path by which the cluster was formed.

In summary, we have demonstrated a new thin-film differential scanning nanocalorimetry technique that is capable of measuring the dynamics of energy exchange at the level of 0.2 nJ. We have shown that the melting point and heat of fusion of nanometer-scale Sn clusters is size dependent and is independent of the process by which the clusters are formed.

REFERENCES

1. M. Takagi, Electron Diffraction Study of Liquid Solid Transition of Thin Metal Films, *J. Phys. Soc. Jpn.*, vol. 9, p. 359, 1954.
2. R. E. Kunz and R. S. Berry, Coexistence of Multiple Phases in Finite Systems, *Phys. Rev. Lett.*, vol. 71, p. 3987, 1993.
3. L. D. Marks, Experimental Studies of Small Particle Structures, *Rep. Prog. Phys.*, vol. 57, p. 603, 1994.
4. C. L. Cleveland and U. Landman, The Energetics and Structure of Nickel Clusters: Size Dependence, *J. Chem. Phys.*, vol. 94, p. 7376, 1991.
5. E. P. Donovan, F. Spaepen, J. M. Poate, and D. C. Jacobson, Homogeneous and Interfacial Heat Releases in Amorphous Silicon, *Appl. Phys. Lett.*, vol. 55, p. 1516, 1989.
6. F. Spaepen and C. V. Thompson, Calorimetric Studies of Reactions in Thin Films and Multiplayers, *Appl. Surf. Sci.*, vol. 38, p. 1, 1989.
7. J. M. E. Harper, Ph.D. thesis, Stanford University, Stanford, CA, 1975.

8. L. A. Clevenger and C. V. Thompson, Nucleation-Limited Phase Selection During Reactions in Nickel/Amorphous-Silicon Multilayer Thin Films, *J. Appl. Phys.*, vol. 67, p. 1325, 1990.
9. S. L. Lai, G. Ramanath, L. H. Allen, P. Infante, and Z. Ma, Heat Capacity of Sn Nanostructures via a Thin-Film Scanning Calorimeter, *Appl. Phys. Lett.*, vol. 70, p. 43, 1997.
10. L. H. Allen and S. L. Lai, Ultra-Sensitive Thin-Film Scanning Calorimeter, Patent Disclosure at UIUC, #T96071, 1996.
11. S. L. Lai, G. Ramanth, L. H. Allen, P. Infante, and Z. Ma, High-Speed (10^4°C/s) Scanning Microcalorimetry with Monolayer Sensitivity (J/m^2), *Appl. Phys. Lett.*, vol. 67, p. 1229, 1995.
12. L. H. Allen, G. Ramanath, S. L. Lai, and Z. Ma, 10^6°C/s Thin Film Electrical Heater: In Situ Resistivity Measurements of Al and Ti/Si Thin Films during Ultra Rapid Thermal Annealing, *Appl. Phys. Lett.*, vol. 64, p. 417, 1994.
13. S. Randzio and W. Zielenkiewicz, Microcalorimeter for Heat of Chemisorption Measurements at Higher Temperature on Evaporated Metallic Films, *Phys. Chem.*, vol. XXIV, p. 323, 1976.
14. C. E. Borroni-Bird and D. A. King, An Ultrahigh Vacuum Single Crystal Adsorption Microcalorimeter, *Rev. Sci. Instrum.*, vol. 62, p. 2177, 1991.
15. A. Stuck, C. E. Wartnaby, Y. Y. Yeo, and D. A. King, Microcalorimetry Study of Ethylene on Pt(110), *Phys. Rev. Lett.*, vol. 74, p. 578, 1995.
16. D. W. Denlinger, E. N. Abarra, K. Allen, P. W. Rooney, M. T. Messer, S. K. Watson, and F. Hellman, Thin Film Microcalorimeter for Heat Capacity Measurements from 1.5K to 800K, *Rev. Sci. Instrum.*, vol. 65, p. 946, 1994.
17. R. E. Cavicchi, G. E. Poirier, J. S. Suehle, M. Caitan, S. Semancik, and D. R. F. Burgess, Pulsed Desorption Kinetics Using Micromachined Microhotplate Arrays, *J. Vacuum Sci. Technol. A*, vol. 12, p. 2549, 1994.
18. D. A. Kyser and R. I. Masel, Design of a Calorimeter Capable of Measuring Heats of Adsorption on Single-Crystal Surfaces, *Rev. Sci. Instrum.*, vol. 58, p. 2141, 1987.
19. K. M. Unruh, B. M. Patterson, and S. I. Shah, Melting Behavior of Sn(SiO_2) Granular Metal Films, *J. Mater. Res.*, vol. 7, p. 214, 1992; K. M. Unruh, T. E. Huber, and C. A. Hubber, Melting and Freezing Behavior of Indium Metal in Porous Glasses, *Phys. Rev. B*, vol. 48, p. 9021, 1993.
20. C. L. Jackson and G. B. McKenna, The Melting of Organic Materials Confined in Porous Solids, *J. Chem. Phys.*, vol. 93, p. 9002, 1990; C. C. Koch, J. S. C. Jang, and S. S. Gross, The Melting Point Depression of Tin in Mechanically Milled Tin and Germanium Powder Mixtures, *J. Mater. Res.*, vol. 4, p. 557, 1989; J. S. C. Jang and C. C. Koch, Melting and Possible Amorphization of Sn and Pb in Ge/Sn and Ge/Pb Mechanically Milled Powders, *J. Mater. Res.*, vol. 5, p. 325, 1990.
21. *American Institute of Physics Handbook*, 3d ed., p. 243, McGraw-Hill, New York, 1972.
22. C. R. M. Wronski, "The Size Dependence of the Melting Point of Small Particles of Tin, *Br. J. Appl. Phys.*, vol. 18, p. 1731, 1967. However, miscalculations might have occurred in obtaining Eq. (3). Such an equation has been rederived in this article.
23. K.-J. Hanszen, Theoretishe Untersuchungen iiber den Schmelzpunkt kleiner Kugelchen, *Z. Phys.*, vol. 157, p. 523, 1960.
24. M. A. Carroll and M. E. Warwick, Surface Tension of Some Sn-Pb Alloys, *Mater. Sci. Technol.*, vol. 3, p. 1042, 1987.
25. D. Turnbull, Formation of Crystal Nuclei in Liquid Metals, *J. Appl. Phys.*, vol. 21, p. 1022, 1955.
26. Y. Lereah, G. Deutscher, P. Cheyssac, and R. Kofman, A Direct Observation of Low-Dimensional Effects on Melting of Small Lead Particles, *Europhys. Lett.*, vol. 12,

p. 709, 1990; P. Kofman, P. Cheyssac, A. Aouaj, Y. Lereah, G. Deutscher, T. Ben-David, J. M. Penisson, and A. Bourret, Surface Melting Enhanced by Curvature Effects, *Surface Sci.*, vol. 303, p. 231, 1994.

27. F. Ercolessi, W. Andreoni, and E. Tosatti, Melting of Small Gold Particles; Mechanism and Size Effects, *Phys. Rev. Lett.*, vol. 66, p. 911, 1991; H. S. Lim, C. K. Ong, and E. Ercolessi, Surfaces Effects in Vibrational and Melting Properties of Pb Clusters, *Z. Phys. D*, vol. 26, p. S45, 1993.
28. J. W. M. Frenken and J. F. van der Veen, Observation of Surface Melting, *Phys. Rev. Lett.*, vol. 54, p. 134, 1985; Pluis, T. N. Taylor, D. Frenkel, and J. F. Van der Veen, Role of Long-Range Interactions in the Melting of a Metallic Surface, *Phys. Rev. B*, vol. 40, 1353, 1989.
29. A. W. Denier van der Gon, R. J. Smith, J. M. Gay, D. J. O'Connor, and J. F. van der Veen, Melting of Al Surfaces, *Surface Sci.*, vol. 227, p. 143, 1990; P. Stoltze, J. K. Norskov, and U. Landman, Disordering and Melting of Aluminum Surfaces, *Phys. Rev. Lett.*, vol. 61, p. 440, 1988.
30. Z. B. Güvenç and J. Jellinek, Surface Melting in Ni, *Z. Phys. D*, vol. 26, p. 304, 1993.
31. R. Garrigos, P. Cheyssac, and R. Kofman, Melting for Lead Particles of Very Small Sizes; Influences of Surface Phenomenon, *Z. Phys. D*, vol. 12, p. 497, 1989.